Optics Letters

Experimental generation of perfect optical vortices through strongly scattering media

Weiming Yuan,[1] Yi Xu,[2,5] Kanpei Zheng,[1] Songnian Fu,[2,3] Yuncai Wang,[2,3] and Yuwen Qin[2,3,4,6]

[1]Department of Electronic Engineering, College of Information Science and Technology, Jinan University, Guangzhou 510632, China
[2]Advanced Institute of Photonics Technology, School of Information Engineering, Guangdong University of Technology, Guangzhou 510006, China
[3]Guangdong Provincial Key Laboratory of Information Photonics Technology, Guangdong University of Technology, Guangzhou 510006, China
[4]Synergy Innovation Institute of GDUT, Heyuan, China
[5]e-mail: yixu@osamember.org
[6]e-mail: qinyw@gdut.edu.cn

Received 30 June 2021; revised 23 July 2021; accepted 26 July 2021; posted 26 July 2021 (Doc. ID 435636); published 20 August 2021

Perfect optical vortices enable the unprecedented optical multiplexing utilizing orbital angular momentum of light, which, however, suffer from distortion when they propagate in inhomogeneous media. Herein, we report on the experimental demonstration of perfect optical vortice generation through strongly scattering media. The transmission-matrix-based point-spread-function engineering is applied to encode the targeted mask in the Fourier domain before focusing. We experimentally demonstrate the perfect optical vortice generation either through a multimode fiber or a ground glass, where the numerical results agree well with the measured one. Our results might facilitate the manipulation of orbital angular momentum of light through disordered scattering media and shed new light on the optical multiplexing utilizing perfect optical vortices.

https://doi.org/10.1364/OL.435636

Optical orbital angular momentum (OAM), originated from a helical phase of electric field $\exp(il\varphi)$, resembles a promising physical dimension of light for optical multiplexing because the states of OAM carrying beams are theoretically unbounded [1–6]. In general, OAM beams of different topological charges manifest themselves as ring-shaped intensity profiles with distinct radius size, which inevitably imposes a fundamental challenge on the coupling between different OAM beams and fiber. At the same time, this property would also restrict the upper limit of spatial density of multiplexing utilizing different OAMs of light. In contrast to a conventional OAM beam, a perfect vortex beam (PVB) can sustain a large topological charge while maintaining a small beam size simultaneously [7], facilitating various interesting science perspectives and attractive applications utilizing PVBs [8–19]. However, both types of OAM beams are fragile when they propagate through strongly scattering media, and a special fiber is needed to sustain such OAM states [4].

Wavefront shaping technologies provide versatile solutions to compensate the scattering destabilization during propagating through such complex scattering media [20–44] and even provide effective means to generate various structured beams through scattering media [20,21,31–33,35,39,40]. To date, conventional OAM beams [31,32], Bessel beams [31,32], helical beams [31], Gaussian beams with tailored polarization [33], and needle beams [35] have been demonstrated experimentally utilizing scattering media. However, the experimental demonstration of PVBs generated upon scattering media, especially utilizing a multimode fiber (MMF) remains the expectation while a promising prospective has not be demonstrated yet. In this Letter, we report on the experimental verification of PVB generation through both a MMF and a ground glass.

As one of the most flexible wavefront shaping techniques, transmission matrix (TM)-based engineering of a light field passing through a scattering medium relies on the measurement of TM for that medium. Because of the linear and deterministic nature of the scattering process even for strongly scattering media, the incident and transmitted light field through a scattering medium can be bridged by a TM, which is defined as the matrix T, whose complex value t_{mn} connects the incident optical field at the mth output mode [charge coupled device (CCD) coordinates (x, y)] to the nth input mode by [22]

$$E_m^{\text{out}} = \sum_{n=1}^{N} t_{mn} E_n^{\text{in}}, \tag{1}$$

where N is the total number of input pixels used in the spatial light modulator (SLM).

Experimentally, the TM can be measured by using full-field interference and four-step phase-shift method [22–27]. Once the TM is calibrated correctly, an encoded phase pattern, which is subsequently used for displaying at the SLM, can be obtained by means of digital optical phase conjugation (DOPC) to produce a focus with a size of diffraction limit at any position of the image plane described in Eq. (1). Inspired by the point-spread-function engineering method [31], it is feasible to tailor the

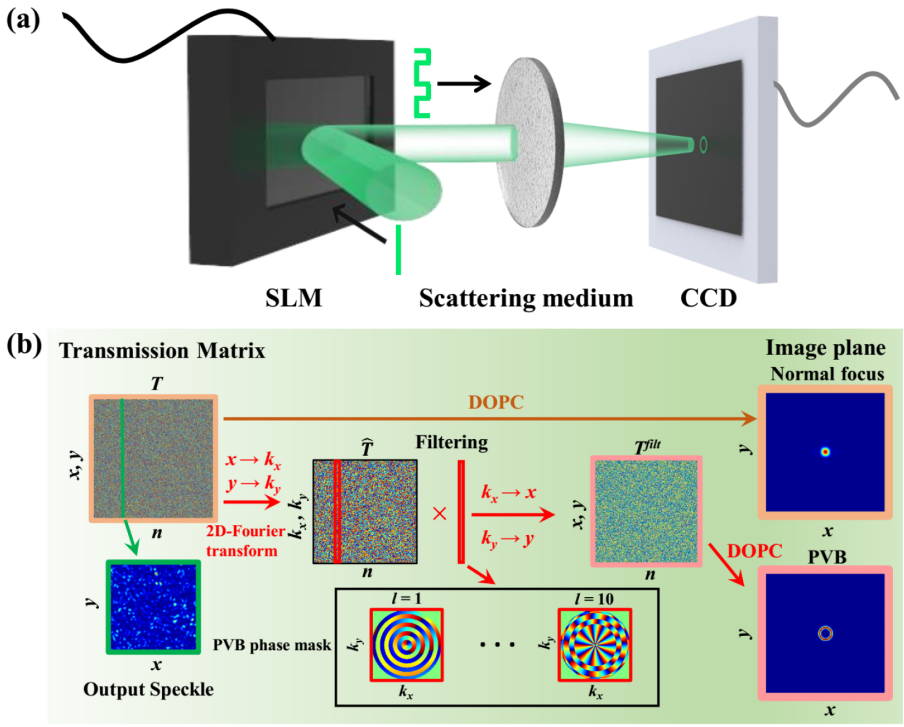

Fig. 1. Proposed mechanism of generating PVBs through a scattering medium. (a) Schematic of the wavefront shaping-based point-spread-function engineering for generating PVBs with different topological charges through a scattering medium. A phase encoded beam by a SLM passes through a scattering medium that can be either a MMF or a ground glass. The transmission beam that experiences multiple scattering in the scattering medium can be tailored to form PVBs at any position of the image plane. (b) Details of procedures to generate PVBs. The TM T is first measured experimentally. Without any filtering in Fourier domain, the DOPC of T can generate a focus with a size of diffraction limit. Here, x and y specify the coordinate of the CCD. With a 2D-Fourier transform of the T, the new TM T^{filt} is obtained by numerically applying a PVB phase mask with an arbitrary topological charge in k-space. After filtering, the DOPC of T^{filt} allows for generating PVBs in the output plane that is recorded by a CCD.

properties of focus by adding a complex mask associated with the characteristics of PVBs in the Fourier domain. Therefore, combining with the theory of PVB, one can generate PVB through a scattering medium by applying wavefront shaping, which is schematically illustrated in Fig. 1(a).

Figure 1(b) presents the mechanism to generate PVBs with arbitrary topological charge through a scattering medium. In principle, the optical field in a virtual pupil can be numerically obtained by performing Fourier transform of the experimentally measured TM for a specified scattering medium, namely, a MMF or a ground glass. The 2D-Fourier transform of the TM T results in $\hat{T}$:

$$\hat{t}_k = \mathcal{F}_{2D}(t_{mn}), \quad m = 1:M, \tag{2}$$

where $\hat{t}$ is one column of $\hat{T}$, n specifies the column number of T, and $k = (k_x, k_y)$ is the wave vector. By numerically filtering the virtual pupil with a topological charge dependent PVB phase mask P_l in k-space and taking the inverse Fourier transform of the filtered matrix, a TM encoded with the information of PVB is obtained. The PVB phase mask can be obtained by using the method proposed by Ostrovsky *et al.* [7], while other methods [8–19] can also be generalized. In polar coordinates, the profile of PVB at a fixed propagation distance with the topological charge l can be expressed by [7]

$$E(\rho, \theta) = \text{circ}\left(\frac{\rho}{R}\right) \exp\left[-\frac{(\rho - \rho_0)^2}{\Delta^2}\right] e^{il\theta}, \tag{3}$$

where ρ_0 and Δ are the radius of the ring and its width, respectively, and R is the radius of the pupil aperture. The PVB phase masks P_l with different topological charges l shown in the inset of Fig. 1(b) correspond to the spatial frequency of Eq. (3) in the k-space. In order to generate PVBs through the scatter medium, we then multiply each column of $\hat{T}$ by the PVB phase mask P_l to obtain a new filtered element in the k-space:

$$\hat{t}_k^{\text{filt}} = \hat{t}_k \times P_l(k_x, k_y). \tag{4}$$

Then, the targeted TM T^{filt} encoded with the PVB of a specified topological charge l can be obtained by performing inverse Fourier transform of Eq. (4):

$$t_{mn}^{\text{filt}} = \mathcal{F}_{2D}^{-1}(\hat{t}_k^{\text{filt}}). \tag{5}$$

Finally, a PVB at any position of output plane can be generated through the scattering medium by applying the DOPC of T^{filt}, whose donut-like intensity profile is independent of topological charge.

In order to verify the validity of the theoretical proposal, we perform numerical simulation of generating PVBs with topological charges ranged from 1 to 10. Based on the linear relationship between incident light and scattered light and the complex Gaussian distributed property of the diffused light [29], we artificially generate the TM by computer to characterize the propagation of light in the scattering medium [29]. We then perform the steps described in Fig. 1(b) to obtain the

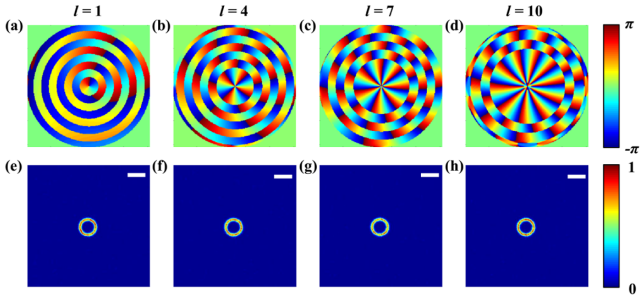

Fig. 2. (a)–(d) PVB phase masks with distinct topological charges l ($l = 1, 4, 7$, and 10) for filtering in the virtual pupil. (e)–(h) Simulation results of the numerically generated PVBs with different topological charges through a scattering medium. The radius of all generated PVBs is independent of topological charge. Scale bar, 100 μm.

PVB phase masks of different topological charges l. Four typical examples ($l = 1, 4, 7, 10$) are shown in Figs. 2(a)–2(d). Here, $\rho_0 = 8L$ and $\Delta = 2L$ are used in Eq. (3), where L is the pixel size of the CCD. We compute the input phase using the DOPC of T^{filt}, and four PVBs with distinct topological charges ($l = 1, 4, 7, 10$) standing over the background in the image plane can be obtained [see Figs. 2(e)–2(h)]. As can be seen from these figures, the intensity profiles of the generated PVB are independent of topological charges. The diameter and radius of the donut-like focus are equal to the targeted ones used in generating the PVB phase masks utilizing Eq. (3) with different topological charges l up to 10.

In order to validate the theoretical results, we perform an experiment of the PVB generation utilizing two typical scattering media. The optical setup for measuring the TM and performing the wavefront shaping is shown in Fig. 3. A semiconductor laser ($\lambda = 532$ nm, MGL-FN-532, Xiai) is filtered and collimated, and a Glan prism is used to produce a horizontally polarized laser beam, which will be effectively modulated by the SLM. Then the incident beam is encoded by a phase-only SLM (PLUTO-NIR, HOLOEYE) with a pre-calculated phase pattern and reflected to the beam splitter. The collimated beam incident on the SLM is divided into two parts, which are corresponding to the modulation part (central square region) and the reference part (outer region), respectively. Then the reflected beam is focused by the objective (Obj2) into the scattering media, which can be either a MMF (Ø400 μm, NA = 0.50, Daheng Optics) or a ground glass (DG10–600, Thorlabs). Another objective (Obj3) is placed behind the scattering medium to collect the scattered light. The output light is then recorded by a CCD (MER-231-41U3C-L, Daheng Imaging). The TMs of two scattering media are both obtained by utilizing full-field interference and four-step phase-shift method [22].

The scenario of a ground glass is investigated first. After completing the TM measurement, the corresponding PVB phase mask of a topological charge l is applied in the numerically filtering step. With the same procedures described in Fig. 1(b), we choose the central pixel of the CCD as the targeted position where the focus locates. Here, the input modes consist of 32×32 macro pixels where each macro pixel indicating an input mode of Eq. (1) is synthesized by 20×20 pixels of the SLM. As a result, 1024 input modes are used in our system. At the same time, we use 256×256 CCD pixels as the output modes. The experimental results of PVBs generated through the ground glass ($l = 1, 4, 7, 10$) are presented in Fig. 4, where

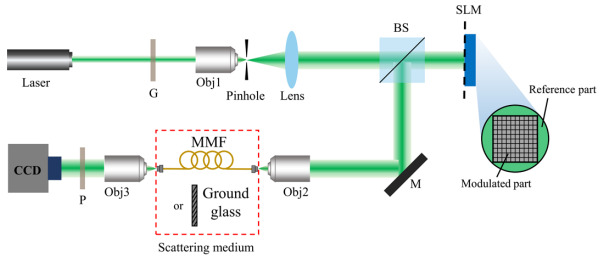

Fig. 3. Experiment setup for generating PVBs through two typical scattering media. G is a Glan prism, P is a linear polarizer, BS is a beam splitter, Obj denotes the microscope objective (Obj1: 40×, NA = 0.65; Obj2: 10×, NA = 0.25; Obj3: 20×, NA = 0.40), and M is a mirror. The Obj1, lens, and pinhole form a spatial filtering and collimating system. A MMF or a ground glass is used here as the scattering medium. The length of MMF is 1 m. The size of pinhole is 20 μm. The focal length of the lens is 100 mm.

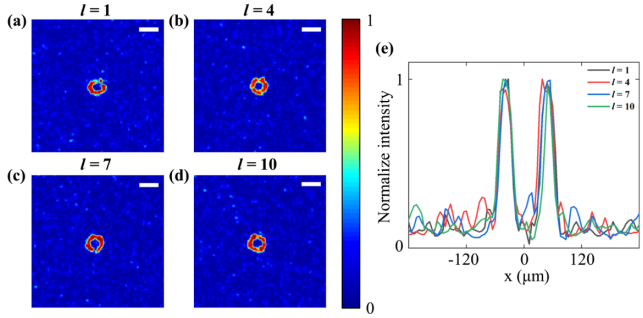

Fig. 4. (a)–(e) Experiment results of PVBs with different topological charge ($l = 1, 4, 7$, and 10) after propagating through a ground glass. Scale bar, 100 μm.

PVBs of distinct topological charges standing over the speckle background are observed. Furthermore, it is clearly revealed that the diameters of four rings are independent of topological charges l [Fig. 4(e)], and the beam profiles of different topological charges are similar to the theoretical analysis shown in Fig. 2. The interference results (data not shown) between the generated PVBs and a Gaussian beam confirm the OAM nature of the generated beams.

Furthermore, MMFs facilitate various applications in optical communication and multiplexing. Because of the inevitable imperfection of fiber geometry and mode coupling, a random speckle pattern appears when a coherent laser beam propagates through a non-polarization maintaining MMF. As a result, it will impose limitations on the applications of MMFs in many fields. Wavefront shaping techniques have been introduced to tailor the optical field transmitted through the MMF [28,32–34,37–42], where the experimental generation of the PVB via a MMF is still absent. By replacing the ground glass with a MMF (1 m) in the experimental setup shown in Fig. 3 while applying similar procedures described above, we can also generate PVBs with different topological charges through a MMF. The experimental results are shown in Fig. 5, where the generated beam profiles of vortex beams with distinct topological charges are similar. It should be pointed out that the experimental results utilizing the MMF are not as good as the ground glass one, which might be due to less precision in calibrating the

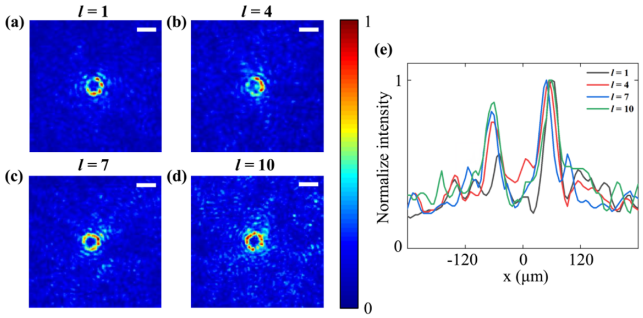

Fig. 5. (a)–(e) Experiment results of PVBs with different topological charges ($l = 1$, 4, 7, and 10) after propagation through a MMF. Scale bar: 100 μm.

corresponding TM because the MMF is more sensitive to the perturbation from environment.

In summary, we propose theoretically and demonstrate experimentally that PVBs with topological charge independent beam profiles can be generated through strongly scattering media. By applying topological charge dependent PVB phase masks to the virtual pupil in Fourier domain, we can generate a PVB at the imaging plane through a MMF or a ground glass. The experimental results agree well with the numerical ones for PVBs with distinct topological charges, where the beam profiles of the generating PVBs are independent of topological charges. The proposed is general for other strongly scattering media whose TM can be measured experimentally. The method can also be generalized to generate PVB array through strongly scattering media [13,14,18]. It is anticipated that the proposed method can become an alternative to generate PVBs through a fiber without applying any modification at the fiber facet, which could increase the coupling efficiency of OAM beams to fiber and might open up new possibilities in an MMF-based endoscope as well as scattering optics.

Funding. National Key Research and Development Program of China (2018YFB1801001); National Natural Science Foundation of China (91750110); Guangdong Introducing Innovative and Entrepreneurial Teams of "The Pearl River Talent Recruitment Program" (2019ZT08X340); Research and Development Plan in Key Areas of Guangdong Province (2018B010114002).

Disclosures. The authors declare no conflicts of interest.

Data Availability. Data underlying the results presented in this paper are not publicly available at this time but may be obtained from the authors upon reasonable request.

REFERENCES

1. L. Allen, M. W. Beijersbergen, R. J. Spreeuwand, and J. P. Woerdman, Phys. Rev. A **45**, 8185 (1992).
2. J. Wang, J. Y. Yang, I. M. Fazal, N. Ahmed, Y. Yan, H. Huang, Y. Ren, Y. Yue, S. Dolinar, M. Tur, and A. E. Willner, Nat. Photonics **6**, 488 (2012).
3. X. Cai, J. Wang, M. J. Strain, B. Johnson-Morris, J. Zhu, M. Sorel, J. L. O'Brien, M. G. Thompson, and S. Yu, Science **338**, 363 (2012).
4. N. Bozinovic, Y. Yue, Y. Ren, M. Tur, P. Kristensen, H. Huang, A. E. Willner, and S. Ramachandran, Science **340**, 1545 (2013).
5. H. Ren, X. Li, Q. Zhang, and M. Gu, Science **352**, 805 (2016).
6. M. L. Chen, L. J. Jiang, and W. Sha, IEEE Antennas Wireless Propag. Lett. **18**, 477 (2019).
7. A. Ostrovsky, C. Rickenstorff-Parrao, and V. Arrizón, Opt. Lett. **38**, 534 (2013).
8. M. Chen, M. Mazilu, Y. Arita, E. Wright, and K. Dholakia, Opt. Lett. **38**, 4919 (2013).
9. J. García-García, C. Rickenstorff-Parrao, R. Ramos-García, V. Arrizón, and A. Ostrovsky, Opt. Lett. **39**, 5305 (2014).
10. P. Vaity and L. Rusch, Opt. Lett. **40**, 597 (2015).
11. Y. Chen, Z. Fang, Y. Ren, L. Gong, and R. Lu, Appl. Opt. **54**, 8030 (2015).
12. V. V. Kotlyar, A. A. Kovalev, and A. P. Porfirev, J. Opt. Soc. Am. A **33**, 2376 (2016).
13. S. Fu, T. Wang, and C. Gao, J. Opt. Soc. Am. A **33**, 1836 (2016).
14. S. Fu, C. Gao, T. Wang, S. Zhang, and Y. Zhai, Opt. Lett. **41**, 5454 (2016).
15. C. Zhang, C. Min, and X. C. Yuan, Opt. Commun. **381**, 292 (2016).
16. J. Mendoza-Hernández, M. Hidalgo-Aguirre, A. I. Ladino, and D. Lopez-Mago, Opt. Lett. **45**, 5197 (2020).
17. C. Rickenstorff, L. del Carmen Gomez-Pavon, C. T. Sosa-Sanchez, and G. Silva-Ortigoza, Opt. Express **28**, 28713 (2020).
18. H. Wang, S. Fu, and C. Gao, Opt. Express **29**, 10811 (2021).
19. Y. Du, D. Liu, S. Fu, Y. Wang, and Y. Qin, Opt. Express **29**, 17353 (2021).
20. I. M. Vellekoop and A. Mosk, Opt. Lett. **32**, 2309 (2007).
21. I. Vellekoop, A. Lagendijk, and A. Mosk, Nat. Photonics **4**, 320 (2010).
22. S. Popoff, G. Lerosey, R. Carminati, M. Fink, A. C. Boccara, and S. Gigan, Phys. Rev. Lett. **104**, 100601 (2010).
23. S. M. Popoff, G. Lerosey, M. Fink, A. C. Boccara, and S. Gigan, New J. Phys. **13**, 123021 (2011).
24. S. M. Popoff, G. Lerosey, M. Fink, A. C. Boccara, and S. Gigan, Nat. Commun. **1**, 81 (2010).
25. H. Yu, T. R. Hillman, W. Choi, J. O. Lee, M. S. Feld, R. R. Dasari, and Y. Park, Phys. Rev. Lett. **111**, 153902 (2013).
26. A. Drémeau, A. Liutkus, D. Martina, O. Katz, C. Schülke, F. Krzakala, S. Gigan, and L. Daudet, Opt. Express **23**, 11898 (2015).
27. J. Yoon, K. Lee, J. Park, and Y. Park, Opt. Express **23**, 10158 (2015).
28. M. Plöschner, T. Tyc, and T. Čižmár, Nat. Photonics **9**, 529 (2015).
29. K. Lee and Y. Park, Nat. Commun. **7**, 13359 (2016).
30. G. Zhu, Y. Chen, Y. Liu, Y. Zhang, and S. Yu, Opt. Lett. **42**, 1257 (2017).
31. A. Boniface, M. Mounaix, B. Blochet, R. Piestun, and S. Gigan, Optica **4**, 54 (2017).
32. C. Ma, J. Di, Y. Zhang, P. Li, F. Xiao, K. Liu, X. Bai, and J. Zhao, Opt. Lett. **43**, 3333 (2018).
33. W. Fan, X. Hu, B. Zhaxi, Z. Chen, and J. Pu, Opt. Express **26**, 7693 (2018).
34. M. Gom, T. B. Norris, E. Michielssen, and R. R. Nadakuditi, Opt. Lett. **43**, 419 (2018).
35. Z. Chen, X. Hu, X. Ji, and J. Pu, IEEE Photon. J. **10**, 6501108 (2018).
36. L. Gong, Q. Zhao, H. Zhang, X. Hu, K. Huang, J.-M. Yang, and Y. Li, Light Sci. Appl. **8**, 27 (2019).
37. Z. Wu, J. Luo, Y. Feng, X. Guo, Y. Shen, and Z. Li, Opt. Express **27**, 5570 (2019).
38. X. Wei, J. C. Jing, Y. Shen, and L. V. Wang, Light Sci. Appl. **9**, 149 (2020).
39. W. Fan, Z. Chen, L. Chen, L. Wu, X. Ji, and J. Pu, IEEE J. Sel. Top. Quantum Electron. **26**, 4400405 (2020).
40. C. Ma, J. Di, J. Dou, P. Li, F. Xiao, K. Liu, X. Bai, and J. Zhao, Appl. Opt. **59**, 701 (2020).
41. G. Huang, D. Wu, J. Luo, Y. Huang, and Y. Shen, Opt. Express **28**, 9487 (2020).
42. Q. Zhao, P. Yu, Y. Liu, Z. Wang, Y. Li, and L. Gong, Appl. Phys. Lett. **116**, 181101 (2020).
43. G. Huang, D. Wu, J. Luo, L. Lu, F. Li, Y. Shen, and Z. Li, Photon. Res. **9**, 34 (2021).
44. Y. Zhou, B. Braverman, A. Fyffe, R. Zhang, J. Zhao, A. E. Willner, Z. Shi, and R. W. Boyd, Nat. Commun. **12**, 1886 (2021).